Cell Reports

Article

Influx-Operated Ca^{2+} Entry via PKD2-L1 and PKD1-L3 Channels Facilitates Sensory Responses to Polymodal Transient Stimuli

Graphical Abstract

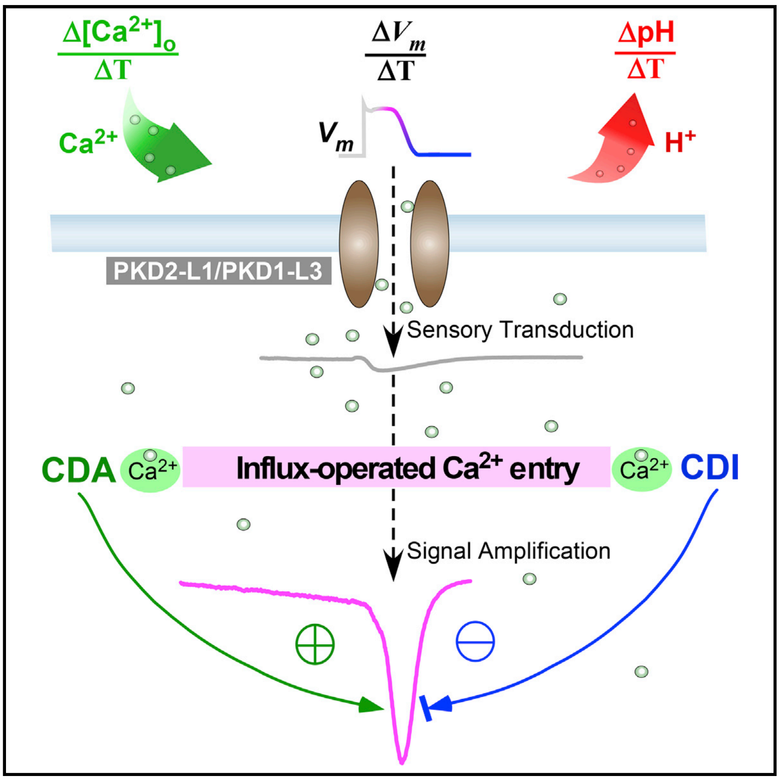

Highlights

- PKD2-L1/PKD1-L3 channel Ca^{2+} influx drives both positive and negative feedback
- Ca^{2+} spikes are inducible when the balance of this feedback is well tuned
- Sensory responses to stimuli with rapid onset/offset are facilitated by Ca^{2+} spikes
- Ca^{2+}-binding EF hands of PKD2-L1 regulate Ca^{2+} feedback and Ca^{2+} spikes

Authors

Mingfeng Hu, Yuxia Liu, Jinzhi Wu, Xiaodong Liu

Correspondence

liuxiaodong@tsinghua.edu.cn

In Brief

Sensing profiles of recombinant PKD2-L1/PKD1-L3 channels challenge their suggested function as molecular transducers. Hu et al. find that influx-operated Ca^{2+} entry can produce Ca^{2+} spikes that augment and reshape sensory responses to polymodal stimuli, including Ca^{2+} exposure, voltage repolarization, and acid withdrawal.

Hu et al., 2015, Cell Reports *13*, 798–811
October 27, 2015
http://dx.doi.org/10.1016/j.celrep.2015.09.041

Influx-Operated Ca^{2+} Entry via PKD2-L1 and PKD1-L3 Channels Facilitates Sensory Responses to Polymodal Transient Stimuli

Mingfeng Hu,[1,4] Yuxia Liu,[1,4] Jinzhi Wu,[1,4] and Xiaodong Liu[1,2,3,*]
[1]X-Lab for Transmembrane Signaling Research, Department of Biomedical Engineering, School of Medicine
[2]School of Life Sciences
[3]IDG/McGovern Institute for Brain Research
Tsinghua University, Beijing 100084, China
[4]Co-first author
*Correspondence: liuxiaodong@tsinghua.edu.cn
http://dx.doi.org/10.1016/j.celrep.2015.09.041

SUMMARY

The polycystic TRP subfamily member PKD2-L1, in complex with PKD1-L3, is involved in physiological responses to diverse stimuli. A major challenge to understanding whether and how PKD2-L1/PKD1-L3 acts as a bona fide molecular transducer is that recombinant channels usually respond with small or undetectable currents. Here, we discover a type of Ca^{2+} influx-operated Ca^{2+} entry (ICE) that generates pronounced Ca^{2+} spikes. Triggered by rapid onset/offset of Ca^{2+}, voltage, or acid stimuli, Ca^{2+}-dependent activation amplifies a small Ca^{2+} influx via the channel. Ca^{2+} concurrently drives a self-limiting negative feedback (Ca^{2+}-dependent inactivation) that is regulated by the Ca^{2+}-binding EF hands of PKD2-L1. Our results suggest a biphasic ICE with opposite Ca^{2+} feedback regulation that facilitates sensory responses to multimodal transient stimuli. We suggest that such a mechanism may also occur for other sensory modalities and other Ca^{2+} channels.

INTRODUCTION

The polycystin subfamily of TRP (TRPP) genes encodes a class of Ca^{2+}-permeable non-selective cation channels (Gees et al., 2010). TRPPs are named after the disease-causing genes TRPP2 (PKD2) and PKD1, mutations in which are responsible for autosomal dominant polycystic kidney disease (ADPKD) (Zhou, 2009). TRPP3 (PKD2-L1) has been linked to various aspects of transmembrane signaling, including sour taste perception and proton-mediated pain (Huang et al., 2006; Huque et al., 2009; Orts-Del'Immagine et al., 2014, 2015), Ca^{2+} homeostasis and sonic hedgehog signaling in primary cilia (DeCaen et al., 2013; Delling et al., 2013), cystic disorders in *Krd* (kidney and retinal defects) mice (Keller et al., 1994), and an aversive response to high salt (Oka et al., 2013). It has been speculated that PKD2-L1/PKD1-L3 channels may act as the sought-after molecular transducers of voltage, Ca^{2+}, pH, heat, and mechanical stress (Chen et al., 1999; Higuchi et al., 2014; Murakami et al., 2005; Shimizu et al., 2009). However, in contrast to prominent Ca^{2+} signals observed in native settings, currents of recombinant PKD2-L1/PKD1-L3 channels in mammalian cells are often very small or undetectable, raising fundamental questions as to whether PKD2-L1 channel complexes indeed function as bona fide transducers to mediate sensory functions in vivo. For example, while data from native preparations support that PKD2-L1 and PKD1-L (PKD1-L1 or PKD1-L3) are involved in mechanosensation of primary cilia (Delling et al., 2013; Murakami et al., 2005; Nauli et al., 2003) and in acid sensing of sour taste (Huang et al., 2006; Kawaguchi et al., 2010), recombinant heteromeric PKD2-L1 channel complexes exhibit little activation in response to physiologically relevant mechanical stress (60 mm Hg or lower) or acid stimuli (pH of 3 or higher) (DeCaen et al., 2013; Inada et al., 2008; Shimizu et al., 2009). Furthermore, PKD2-L1 sensitivity to transmembrane potentials (V_m) is poor as inward currents are small and have weak voltage dependence (Ishimaru et al., 2006), arguing against an important role in action potential-related Ca^{2+} signaling (Orts-Del'Immagine et al., 2014, 2015; Wu et al., 1998). Another signal, extracellular Ca^{2+}, might also act as the stimulus that activates PKD2-L1 in taste cells or primary cilia as postulated (Delling et al., 2013; Tordoff, 2001). Indeed, exposure to high concentrations of extracellular Ca^{2+} ($[Ca^{2+}]_o$) was reported to activate homomeric PKD2-L1 channels reconstituted in *Xenopus* oocytes, giving rise to an inward Ca^{2+} current that displayed inactivation (Chen et al., 1999; Zheng et al., 2015). Unfortunately, such Ca^{2+}-activated Ca^{2+} current (I_{Ca}) responses have not been observed for either homomeric or heteromeric PKD2-L1 channels overexpressed in mammalian cells (DeCaen et al., 2013).

Here, we examine activities of recombinant PKD2-L1/PKD1-L3 channels in HEK293 cells in response to transient Ca^{2+}, V_m, or acid stimuli. We report the discovery and analyses of a type of Ca^{2+} spike that is autonomously controlled by Ca^{2+} influx through the channel (influx-operated Ca^{2+} entry or ICE). We suggest that ICE may occur in other sensory contexts and other physiological functions.

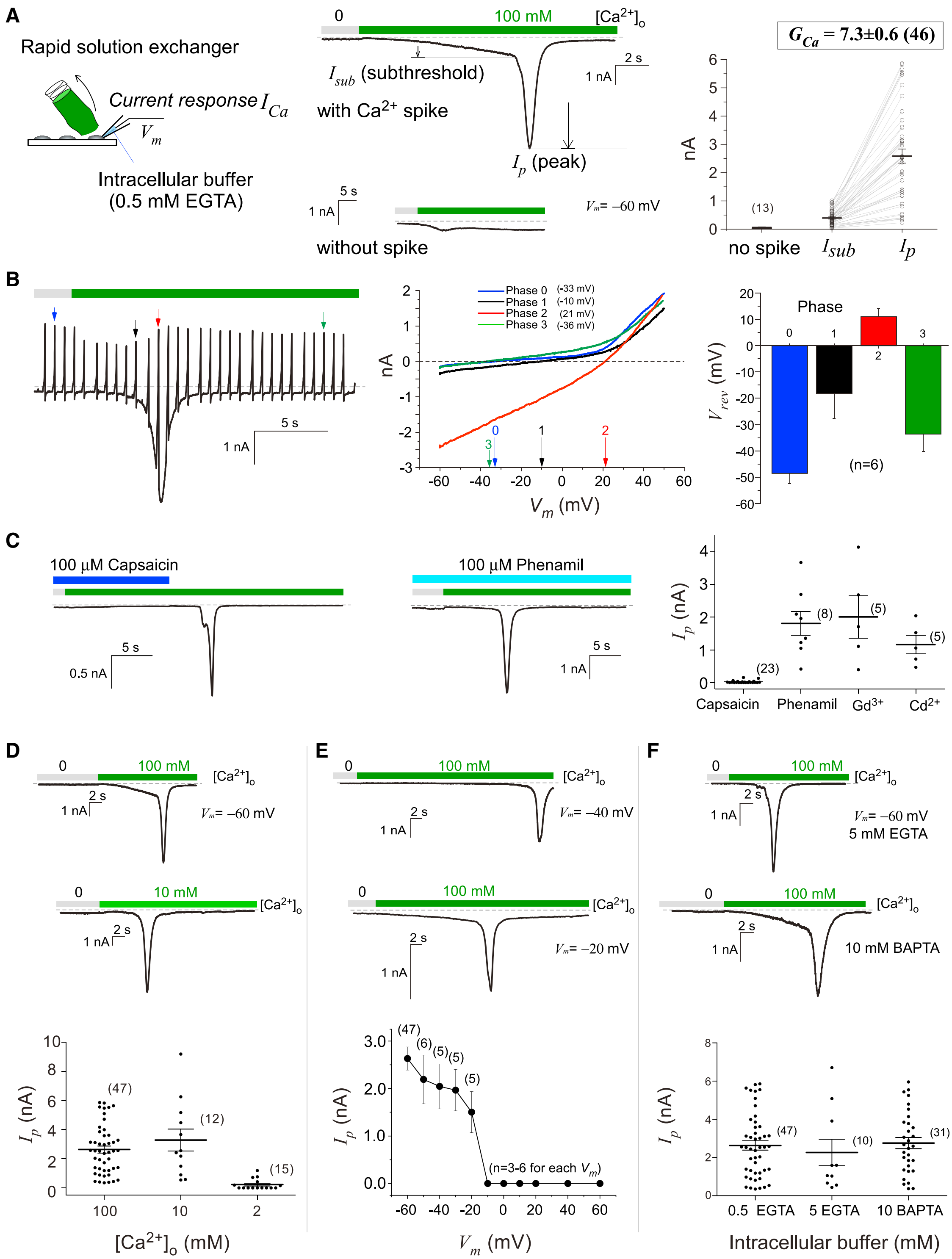

Figure 1. Ca^{2+} Spikes from PKD2-L1/PKD1-L3 Channels Are Induced by Ca^{2+} Exposure

(A) Ca^{2+} spikes from PKD2-L1/PKD1-L3. Representative whole-cell recording of I_{Ca} with or without Ca^{2+} spikes when $[Ca^{2+}]_o$ was quickly switched from 0 to 100 mM, with ~100 ms to completely switch the solutions. Peak currents (I_p) of Ca^{2+} spike (2.6 ± 0.2 nA, n = 47) and the gain ($G_{Ca} = I_p/I_{sub}$) for rapid Ca^{2+} exposure protocol (7.3 ± 0.6, n = 46) were estimated (mean ± SEM) under standard experimental conditions: V_m = −60 mV, 100 mM $[Ca^{2+}]_o$ exposure, and 0.5 mM EGTA included in pipettes, unless otherwise indicated.

(legend continued on next page)

RESULTS

Induction of Ca^{2+} Spikes by Rapid Ca^{2+} Exposure

PKD2-L1 and PKD1-L3 were co-expressed in mammalian cell lines to test whether high Ca^{2+} stimuli could produce a similar response to pronounced I_{Ca} from homomeric PKD2-L1 channels in oocytes (Chen et al., 1999). In initial trials, only a very small response was elicited by 100 mM Ca^{2+} via a regular (slow) bath perfusion system (Figure S1A). Surprisingly, upon a much faster Ca^{2+} exposure, i.e., a 100-mM step by rapid solution exchanger, we recorded nA-sized I_{Ca} (2.6 ± 0.2 nA, n = 47) in 45% of patched HEK293 cells (Figure 1A), and similarly in Chinese hamster ovary (CHO) cells (Figure S2B). In most traces, following an initial brief suppression and a subsequent gradual deflection, an inward current got accelerated at some threshold, rapidly peaked, and then inactivated, altogether forming a Ca^{2+} spike-like response (Figure 1A). Such I_{Ca} with Ca^{2+} spike essentially facilitates responses to external stimuli: the small response of early subthreshold phase is dramatically amplified into a Ca^{2+} spike. To quantify this amplification, we define a gain factor (G_{Ca}) as the ratio of the peak of the Ca^{2+} spike to the amplitude of the subthreshold current (G_{Ca} = 7.3 ± 0.6, n = 46).

Ca^{2+} entry during the Ca^{2+} spike was confirmed by patch recording and simultaneous Ca^{2+} imaging with GCaMP3, a genetically encoded Ca^{2+} sensor (Figures S2I and S2J). The reversal potential (V_{rev}) during the Ca^{2+} spike was positively shifted, consistent with an increase of Ca^{2+} conductance (Figures 1B and S3). The relative permeability of Ca^{2+} versus Na^+ was estimated (P_{Ca}/P_{Na} = 5.3 ± 0.7, n = 10) by switching Ca^{2+} solution to Na^+ solution during Ca^{2+} spikes (Figure S3), consistent with the documented values (about 4–11) (Chen et al., 1999; DeCaen et al., 2013; Inada et al., 2008).

Ca^{2+} spikes appear to be specific to PKD2-L1/PKD1-L3, as no spikes were observed from either PKD2-L1 expressed alone in HEK293 cells or any other cDNA combinations that we tested (Figure S2F). When the N terminus of PKD1-L3 was truncated, Ca^{2+} spikes also became absent (Figure S4). To further confirm that PKD2-L1/PKD1-L3 mediates I_{Ca} spikes, we added 100 μM capsaicin, a known antagonist of the channel complex (Ishii et al., 2012), which reversibly blocked the Ca^{2+} spike (Figure 1C). We examined the potential role of stimulus strength $[Ca^{2+}]_o$ (Ishii et al., 2012), membrane potential V_m (Ishimaru et al., 2006), intracellular buffers, and the speed of transient stimuli $\Delta[Ca^{2+}]_o/\Delta T$. I_{Ca} spikes were clearly identified for $[Ca^{2+}]_o \geq 10$ mM, suggesting a mechanism of Ca^{2+}-dependent activation (CDA) (Figure 1D). Ca^{2+} spikes could be induced at $V_m \leq -20$ mV but were absent at $V_m \geq -10$ mV, exhibiting apparent inward rectification (Figure 1E). Notably, I_{Ca} spikes recorded with 0.5 mM EGTA, 5 mM EGTA, or 10 mM BAPTA are indistinguishable (Figure 1F). This contrasts with eliminated Ca^{2+} response from homomeric PKD2-L1 in oocytes by EGTA at mM concentrations (Chen et al., 1999). This difference might be due to active participation of PKD1-L3 in pore formation and ion permeation of the channel complex (Yu et al., 2012). Such buffer insensitivity of PKD2-L1/PKD1-L3 suggests that Ca^{2+} spikes are likely not triggered by an increase of bulk cytosolic Ca^{2+}. Consistent with this, Ca^{2+} spikes could not be induced by intracellular Ca^{2+} ($[Ca^{2+}]_i$) elevations achieved via either store depletion or pipette delivery (Figure S5). The probability of eliciting a Ca^{2+} spike varied according to the speed of Ca^{2+} exposure: the slower the rate of change (or the longer transient time ΔT), the less likely it became to trigger Ca^{2+} spikes. At the slowest speed to achieve $\Delta[Ca^{2+}]_o$ by bath perfusion ($\Delta T \geq 120$ s), no spikes were elicited (Figure 2A). The dependence of spike generation on the time rate of Ca^{2+} stimuli ($\Delta[Ca^{2+}]_o/\Delta T$) rather than just $[Ca^{2+}]_o$ or $\Delta[Ca^{2+}]_o$ is inconsistent with a simple extracellular mechanism of CDA.

Induction of Ca^{2+} Spikes by V_m Repolarization

We devised a voltage protocol, mimicking action potentials, where the time rate of V_m repolarization was varied using different ramping speeds (Figure 2B). V_m repolarization produced pronounced Ca^{2+} spikes, resembling those obtained with fast Ca^{2+} exposure. However, Ca^{2+} spikes were absent when the speed of repolarization was substantially slowed down ($\Delta T \geq 120$ s for ΔV_m = 80 mV). In the case of high $[Ca^{2+}]_o$ built up by slow bath perfusion, which itself was unable to trigger spikes (Figure S1A), an instantaneous V_m drop induced Ca^{2+} spikes (Figure 2C). These results suggest that the kinetics of Ca^{2+} influx or the speed of Ca^{2+} entry is critical to trigger Ca^{2+} spikes. If so, Ca^{2+} exposure and V_m repolarization essentially may share a similar mechanism of action for triggering Ca^{2+} spikes.

The notion of common mechanism is further supported by the fact that the latency to induce spikes (T_p, defined in Figure S2A) for either rapid ΔV_m or $\Delta[Ca^{2+}]_o$ was comparable (~12 s). Similar to G_{Ca}, a gain factor of G_{Vm} can be defined and estimated (14.3 ± 5.5, n = 8) to quantify the amplification by repolarization-induced Ca^{2+} spikes. The value of the conditioning voltage step preceding repolarization (pre-drop V_m) strongly influenced the induction of Ca^{2+} spike. An instantaneous repolarization (ΔV_m = 80 mV) failed to trigger Ca^{2+} spikes when the conditioning voltage step was set to −60 or −30 mV (Figure 2D). Ca^{2+} influx through the channel during the conditioning step could lead to

(B) Reversal potentials measured at different I_{Ca} phases. *I-V* curves were obtained from voltage ramps (from −60 mV to +50 mV of 100-ms durations) at 500-ms intervals, by which V_{rev} values were determined (n = 6 cells): pre-exposure phase "0," −48.6 ± 3.8 mV; subthreshold phase "1," −18.1 ± 9.6 mV; Ca^{2+}-spike phase "2," 11.1 ± 3.1 mV; and inactivation phase "3," −33.6 ± 6.6 mV (mean ± SEM). More details are available in Figure S3.

(C) Blockage of Ca^{2+} spikes by compounds. 100 μM capsaicin blocked Ca^{2+} spikes, which was subsequently washed off (n = 3). 100 μM of phenamil, $GdCl_3$, and $CdCl_2$ all failed to block.

(D) I_{Ca} with different $[Ca^{2+}]_o$. 10 mM or higher $[Ca^{2+}]_o$ triggered I_{Ca} spikes (3.3 ± 0.7 nA, n = 12) (mean ± SEM), whereas 2 mM $[Ca^{2+}]_o$ only produced rather mild responses without major characteristics of Ca^{2+} spike.

(E) Tests with different holding V_m. I_{Ca} traces with Ca^{2+} spikes when V_m was held at −40 mV (upper, 2.0 ± 0.5 nA, n = 5) or −20 mV (lower, 1.5 ± 0.4 nA, n = 6) (mean ± SEM). In contrast, when $V_m \geq -10$ mV, I_{Ca} spikes failed to get triggered (totally 24 cells).

(F) Tests with different intracellular Ca^{2+} buffers. For intracellular buffers of 5 mM EGTA (upper) or 10 mM BAPTA (lower), instead of 0.5 mM EGTA as in (A)–(F), I_{Ca} spikes: 0.5 mM EGTA (2.6 ± 0.2 nA, n = 47), 5 mM EGTA (2.3 ± 0.7 nA, n = 10), and 10 mM BAPTA (2.8 ± 0.3 nA, n = 31) (mean ± SEM).

See also Figure S2.

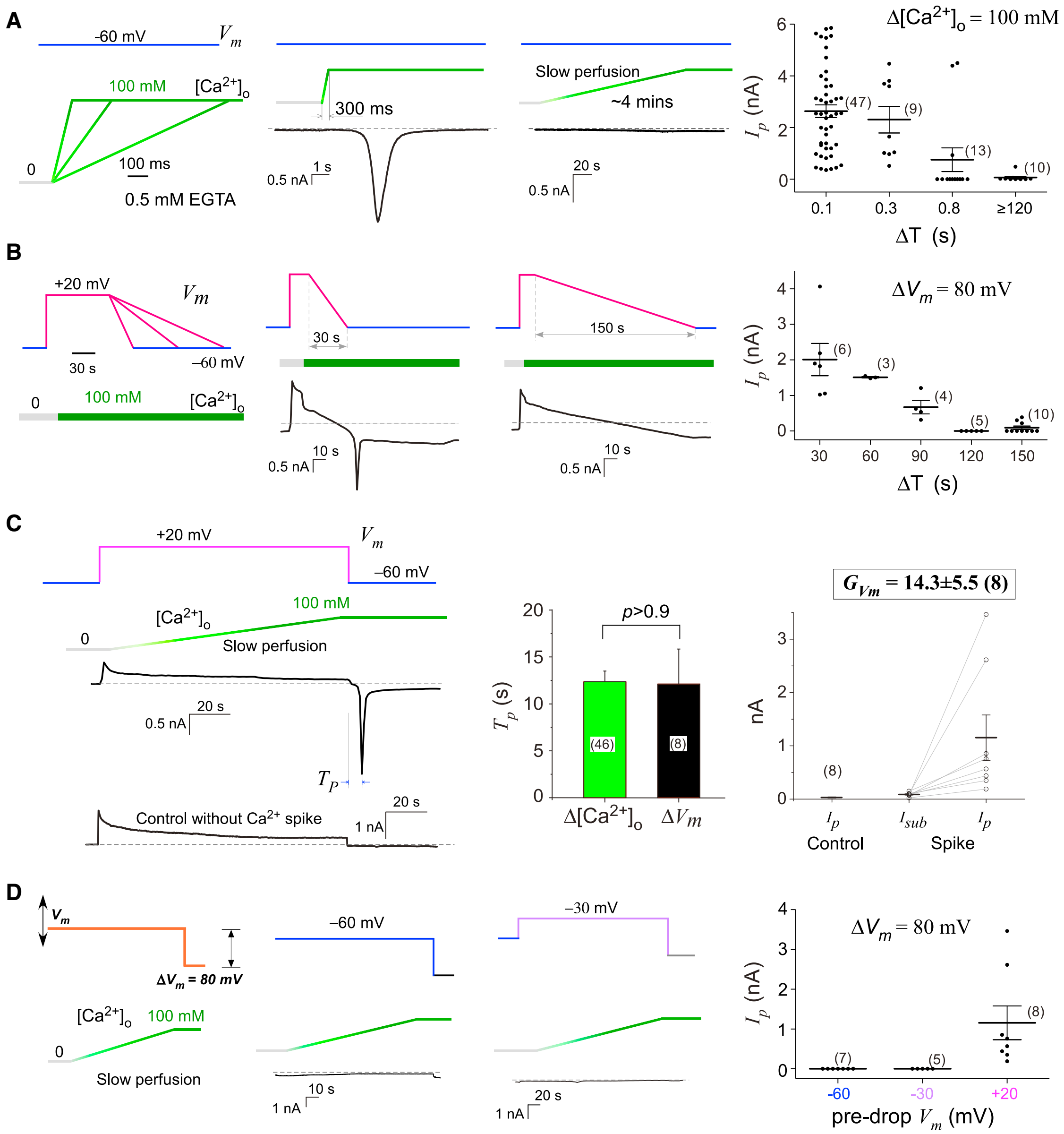

Figure 2. V_m Repolarization Triggers Ca^{2+} Spikes

(A) Speed dependence of Ca^{2+} exposure. I_{Ca} spikes could be triggered by rapid $\Delta[Ca^{2+}]_o$ of 100 mM (transient time $\Delta T \leq$ 800 ms achieved by rapid solution exchanger) but not by slower Ca^{2+} perfusion (ΔT = 2–4 min via chamber perfusion).

(B) Speed dependence of V_m repolarization. V_m was held at a positive level of +20 mV before 100 mM Ca^{2+} perfusion. If subsequent V_m drop (ΔV_m = 80 mV) was fast enough ($\Delta T \leq$ 90 s), Ca^{2+} spikes were inducible, as compared with slower V_m drop ($\Delta T \geq$ 120 s), which failed to trigger spikes.

(C) Signal amplification revealed by V_m drop. Slow (bath) perfusion of 100 mM Ca^{2+} was applied when V_m was held at +20 mV. Ca^{2+} spikes were induced following ΔV_m of 80 mV (eight out of 16 cells in total). T_p time here by ΔV_m was comparable to that by $\Delta[Ca^{2+}]_o$ in Figure 1A ($p > 0.9$). Gain factor of G_{Vm} was estimated (14.3 ± 5.5, n = 8) (mean ± SEM).

(D) Pre-drop V_m and Ca^{2+} spikes. For the same V_m drop (ΔV_m = 80 mV), pre-drop V_m of +20 mV was able to trigger I_{Ca} spikes as in (C), but no spike was observable when pre-drop V_m was set to −60 mV or −30 mV.

Ca^{2+}-dependent inactivation (CDI) (Chen et al., 2015; Inada et al., 2008), which would be expected to impair CDA and prevent spikes. Conditioning voltage steps above the reversal potential would avoid such unfavorable Ca^{2+} influx and be permissive for CDA and spikes. Rapid Ca^{2+} influx across plasma membrane implemented by voltage-gated Ca^{2+} channels (Ca_V) or light-sensitive Ca^{2+} permeable channels (CatCh) did not induce I_{Ca} spikes, nor did direct delivery of high $[Ca^{2+}]_i$ (up to 2 mM) through recording pipettes (Figure S5). These results argue that the determinant of spike induction is Ca^{2+} either passing through or exiting from the pore of PKD2-L1/PKD1-L3 channels and cannot be achieved by other sources of Ca^{2+}.

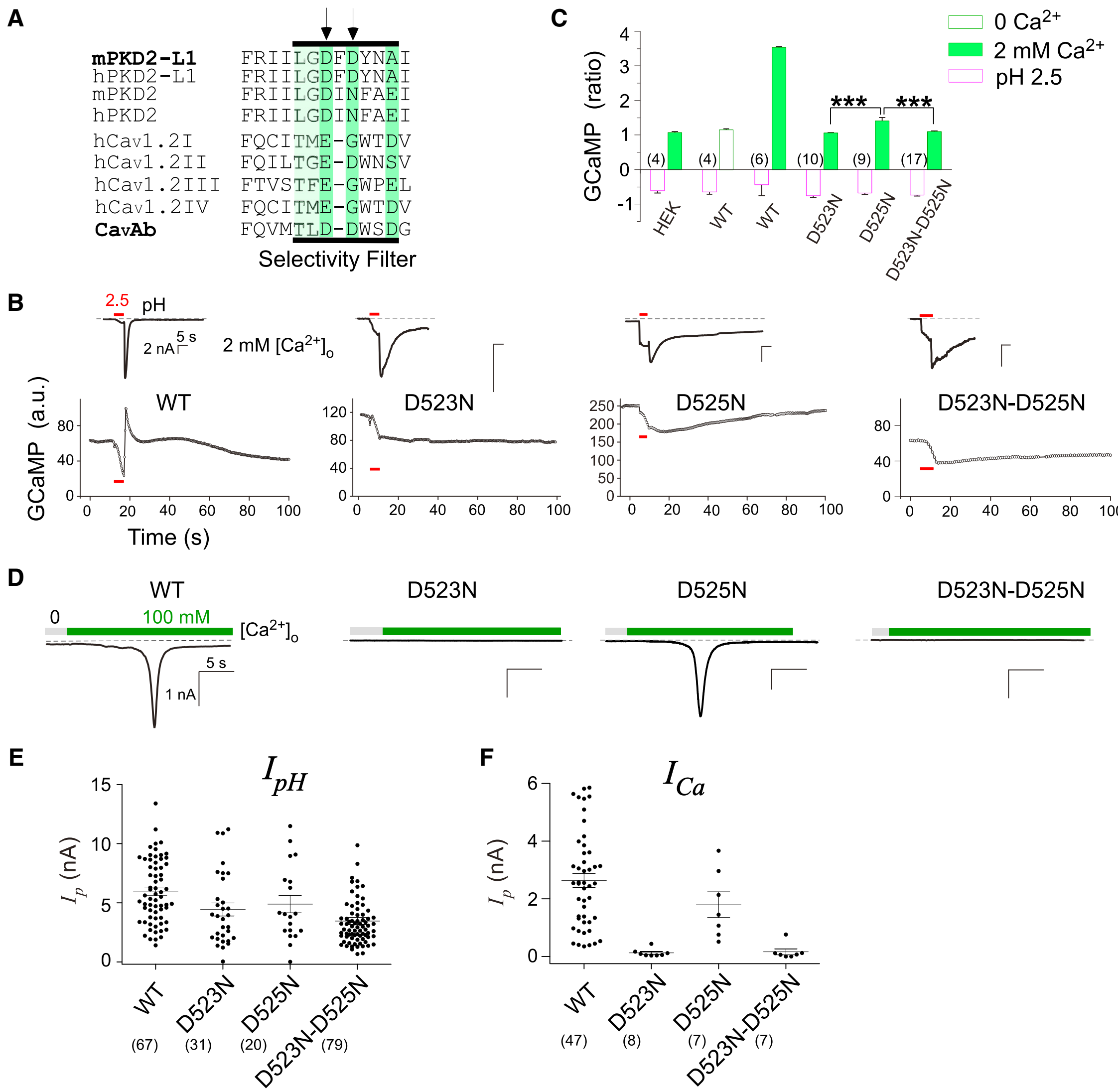

Figure 3. Ca^{2+} Influx Underlies Ca^{2+} Spikes

(A) Sequence alignment of selectivity filters with the two pore mutations of PKD2-L1 indicated. The critical residues for Ca^{2+} selectivity are in dark- or light-green shades.

(B) Simultaneous monitoring of current and Ca^{2+} for I_{pH}. GCaMP3 fluorescence intensity (a.u.) was examined in HEK cells expressing WT PKD2-L1 or pore mutants with D523N and/or D525N. Ca^{2+} dynamics was indicated by fluorescence changes following the initial decrease due to proton quenching (Figure S2I). Red bar represents the application of acid stimuli at a pH of 2.5. Experimental conditions: $V_m = -60$ mV, 2 mM $[Ca^{2+}]_o$ and 5 mM intracellular EGTA.

(C) Summary of Ca^{2+} fluorescence associated with I_{pH}. $[Ca^{2+}]_i$ was quantified by ratio of fluorescence change. Acid applications directly caused fluorescence inhibitions, indistinguishable among all cases. Fluorescence increases reflect Ca^{2+} influx via I_{pH} : HEK control (1.08 ± 0.03, n = 4), WT PKD2-L1/PKD1-L3 in 0 mM $[Ca^{2+}]_o$ (1.18 ± 0.03, n = 4); WT (3.53 ± 0.03, n = 6), D523N (1.05 ± 0.01, n = 10), D525N (1.41 ± 0.10, n = 9), and D523N-D525N (1.10 ± 0.02, n = 17) in 2 mM $[Ca^{2+}]_o$ (in ratio, mean ± SEM, ***$p < 0.001$).

(D) Effects of pore mutation. Mutations of D523N and D523N-D525N did not produce Ca^{2+} spikes, but D525N with residue Ca^{2+} permeability as shown in (C) did generate I_{Ca} spikes.

(E and F) Summary of I_{pH} and I_{Ca} recordings. All pore domain mutants similarly produced I_{pH} : WT PKD2-L1/PKD1-L3 (5.9 ± 0.3 nA, n = 67), D523N (4.1 ± 0.3 nA, n = 31), D525N (4.9 ± 0.7 nA, n = 20), and D523N-D525N (3.5 ± 0.3 nA, n = 79). Only WT (2.6 ± 0.2 nA, n = 47) and D525N (1.8 ± 0.4 nA, n = 7) were able to produce I_{Ca} spikes (mean ± SEM).

See also Figure S5.

Ca^{2+} Influx Autonomously Triggers Ca^{2+} Spikes

To test the notion that Ca^{2+} influx through the PKD2-L1/PKD1-L3 channel is required to induce Ca^{2+} spikes, we mutated the two aspartate residues in the pore (D523N and D525N) that are critical for Ca^{2+} permeability (Fujimoto et al., 2011; Tang et al., 2014; Yu et al., 2012) (Figure 3A). First, we performed GCaMP-based Ca^{2+} imaging to validate the pore mutations (Figure 3B). In response to strong acid (pH 2.5), PKD2-L1/PKD1-L3 channels would not produce much onset current; however, as soon as the acid was withdrawn, a pronounced inward current was triggered by the rapid change (offset) of pH, known as off response (I_{pH}) (Inada et al., 2008). GCaMP fluorescence associated with I_{pH} of D523N or D523N-D525N mutants exhibited nearly no change. Ca^{2+} fluorescence from D525N, though impaired, was significantly higher than other mutants, indicating incomplete blockage of Ca^{2+} influx (Figure 3C). All mutant channels are functional as confirmed by their I_{pH} (Figure 3E), but with different abilities to produce I_{Ca} spikes that positively correlate with their relative Ca^{2+} permeabilities (Figures 3D and 3F). Hence, substantial Ca^{2+} influx via the channel is both necessary and sufficient for spike induction, which represents a unique form of autonomous CDA.

EF Hands of PKD2-L1 Profoundly Affect Ca^{2+} Spikes

The importance of Ca^{2+} in channel activation was further demonstrated by the rising speed (t_r) of I_{Ca} spikes (Figure S2A). With weak intracellular buffer of 0.5 mM EGTA, I_{Ca} spikes induced by 100 mM Ca^{2+} exhibited much faster t_r compared with those elicited with 10 mM Ca^{2+} (Figure 4A). Putative Ca^{2+} binding sites might lie in EF hands at the carboxyl terminus of PKD2-L1. A structural model of EF-hand motifs of PKD2-L1 was computationally achieved based on the homology to EF hands of PKD2 (Petri et al., 2010) and canonical EF hands of calmodulin (CaM) (Figure 4B). In addition to a highly conserved EF2 domain, EF1 domain of PKD2-L1 might also participate in channel regulations by Ca^{2+}. Indeed, mutants featuring deletion of EF1, EF2, or both turned into faster channels (Figure 4C). Such a facilitatory role of EF hands in CDA was made more evident by 2 mM $[Ca^{2+}]_o$ exposure: wild-type (WT) channels (mPKD2-L1/PKD1-L3) failed to produce any definitive Ca^{2+} spike (Figure 4D); in contrast, the same protocol readily triggered Ca^{2+} spikes from mutant channels with EF-hand deletions.

Channel Inactivation Is Fully Ca^{2+} Dependent

Homomeric PKD2-L1 channels are subject to CDI subsequent to channel activation (Chen et al., 1999). Similar CDI has also been observed in acid-evoked I_{pH} of PKD2-L1/PKD1-L3 (Chen et al., 2015; Inada et al., 2008). Our data demonstrated that the decay time (t_d, Figure S2A) of I_{Ca} was significantly faster with high $[Ca^{2+}]_o$ 100 mM (Figure 5A). To avoid complications arising from the opposite effects of CDI and CDA, we focused instead on inactivation of I_{pH} provided that I_{Ca} and I_{pH} undergo similar CDI. Inactivation of I_{pH} was confirmed to be highly regulated by $[Ca^{2+}]_o$ in the range from 0 to 100 mM (Figure 5B) and sensitive to intracellular Ca^{2+} buffers of different strength (Figure 5C). To examine the dependence of inactivation on Ca^{2+}, we used a combination of strongly buffered $[Ca^{2+}]_i$ (10 mM BAPTA) and 0 $[Ca^{2+}]_o$, which completely abolished the inactivation in 12 out of 27 cells, converting the decay into a "flat" phase (Figure 5E). Such elimination of inactivation suggests a completely Ca^{2+}-dependent phenomenon and also firmly excludes an extracellular contribution to the CDI. Dual mutations of D523N and D525N in the pore domain uncovered the full Ca^{2+} dependence of I_{pH} inactivation (summarized in Figure 5G). Even with 2 mM $[Ca^{2+}]_o$ present, a number of I_{pH} traces (10 out of 33, Figure 5F) of the mutant channel exhibited ultra-slow inactivation, similar to that observed under Ca^{2+}-free conditions (Figure 5E).

Collectively, strong intracellular buffers can attenuate but not eliminate CDI, unless Ca^{2+} influx through the channel is also knocked out. Key sites underlying CDI may include residues along permeation pathway and/or of the cytosolic motifs. Within such CDI scheme, we analyzed putative Ca^{2+}-binding motifs on PKD2-L1 (Figure 4B). Mutagenesis suggested that EF hands are directly linked to CDI (Figure 5H) by binding Ca^{2+}, as CDI can be substantially attenuated by point mutations of E613A in EF1, D643A in EF2, dual mutations of ED/AA, and by deletions of ΔEF1 or ΔEF2. All these mutants are functionally capable of producing I_{Ca} and I_{pH} with indistinguishable amplitudes (Figure S6).

Further Manifestations of ICE with Channel Variants and Acid Sensing

As unveiled by our data and analyses, Ca^{2+} spikes are essentially operated by CDA and CDI, both of which are tightly controlled by Ca^{2+} influx through the channel; therefore, we also termed this phenomena as ICE. Most experiments along the way to discover ICE were conducted with mPKD2-L1, originally cloned from mouse taste receptor cells (TRC) (Ishimaru et al., 2006). However, PKD2-L1 is widely expressed in a variety of tissues and organs, encoded by differential splice variants. Human PKD2-L1 (hPKD2-L1) reportedly has at least three other splice variants, cloned from kidney, liver, or testis, respectively (Li et al., 2002). We examined whether the key aspects of ICE revealed from mPKD2-L1 would be applicable to hPKD2-L1 variants. Sequence alignments indicate that these genes share high homology (Figure S7), except for a few discrepancies, e.g., hPKD2-L1_Liver lacks EF2. In spite of sequence differences, all four isoforms similarly produced pronounced responses upon Ca^{2+} exposure or acid withdrawal (Figure S7), except that hPKD2-L1_Liver exhibited weaker CDI (slower decay in I_{pH}) than hPKD2-L1_Kidney (Figure 6A). The critical role of EF2 motif in ICE also manifested itself with hPKD2-L1 variants; when exposed to 10 mM $[Ca^{2+}]_o$, the liver variant produced ICE spikes, whereas the kidney variant did not (Figure 6B).

One major concern relating to recombinant PKD2-L1/PKD1-L3 channels is that the sensing threshold is very acidic (very small I_{pH} for pH = 3), in comparison with native responses (Figure S1C). We found that when the balance between CDA and CDI was appropriately tuned, even though the initial acid response (the first peak) might be small, the subsequent ICE and resulted spikes (the second peak) could offer substantial signal amplifications (gain factor of G_{pH}: 13.9 ± 2.6, n = 12) (Figure 6C). Ca^{2+} spikes here should be directly triggered by Ca^{2+} influx via I_{pH} other than prior Ca^{2+} exposure, since T_p latency associated with ΔpH was significantly shorter ($p < 0.001$) than that with $\Delta[Ca^{2+}]_o$. ICE amplification can make striking differences in acid sensitivity for the same channel as demonstrated by mPKD2-L1_ΔEF1-EF2 (Figure 6D). Upon acid (pH = 3) withdrawal in 0 $[Ca^{2+}]_o$, only small I_{pH} can be observed from the mutant channel, similar to WT mPKD2-L1; in contrast, under the same conditions except for $[Ca^{2+}]_o$ changed to 2 mM, surprisingly large I_{pH} responses were elicited through ICE-mediated Ca^{2+} spikes, more clearly evidenced as the second peaks in some traces. Ca^{2+} sensitized channels (but not the mutant of

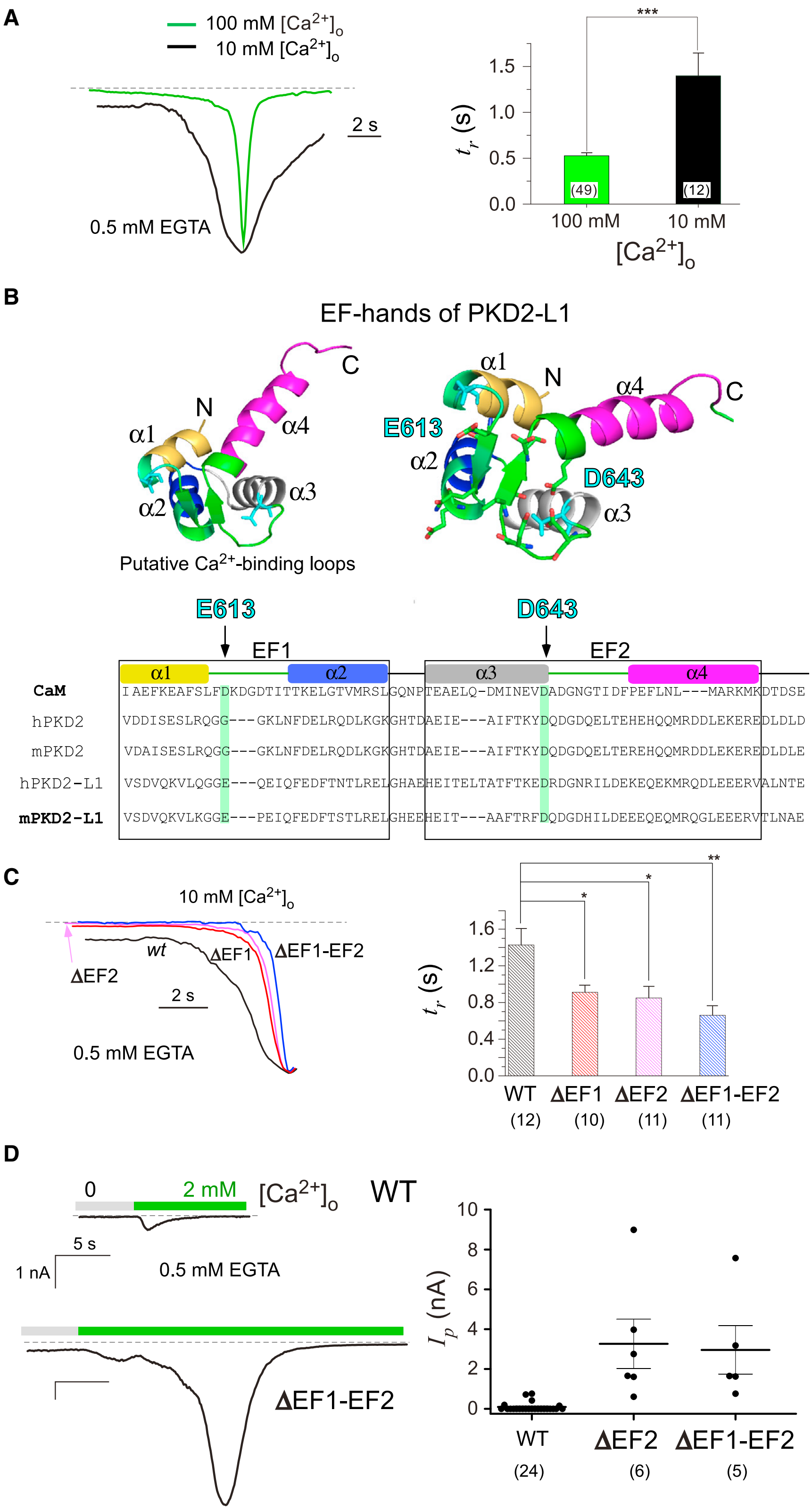

Figure 4. EF Hands Affect CDA of Ca^{2+} Spikes

(A) Speed of rising phase with different $[Ca^{2+}]_o$. I_{Ca} traces were normalized and compared for 100 and 10 mM $[Ca^{2+}]_o$ exposure (left). Statistical summary (right): t_r with 100 mM $[Ca^{2+}]_o$ (0.53 ± 0.03 s, n = 49), significantly different from t_r with 10 mM $[Ca^{2+}]_o$ (1.43 ± 0.18 s, n = 12) (mean ± SEM, ***$p < 0.001$).

(B) Homology modeling for EF hands of PKD2-L1. The homology structure was predicated by computational modeling, based on the alignment of EF-hand sequences from CaM, PKD2, and PKD2-L1 of mouse and/or human. The EF hands between two α-helixes are putative Ca^{2+}-binding loops.

(C) EF-hand deletions slowed down t_r. I_{Ca} traces from EF-hand mutants were normalized and compared. Statistical summary of t_r values for channel complexes: WT (1.43 ± 0.18 s, n = 12), ΔEF1 (0.91 ± 0.08 s, n = 10), ΔEF2 (0.85 ± 0.13 s, n = 11), and ΔEF1-EF2 (0.66 ± 0.10 s, n = 11) (mean ± SEM, *$p < 0.05$, **$p < 0.005$). Experimental conditions: V_m = −60 mV, 0.5 mM EGTA, and 10 mM $[Ca^{2+}]_o$.

(D) EF-hand deletions and Ca^{2+}-spike induction. EF-hand deletions unveiled I_{Ca} spikes with 2 mM $[Ca^{2+}]_o$ (lower left, ΔEF1-EF2 mutant), but no spike with WT PKD2-L1/PKD1-L3 (upper left). Statistical summary (right): ΔEF2 mutant (3.3 ± 1.2 nA, n = 6) and ΔEF1-EF2 mutant (3.0 ± 1.2 nA, n = 5) (mean ± SEM); in contrast, WT channels failed to elicit I_{Ca} spikes (n = 24).

See also Figure S6.

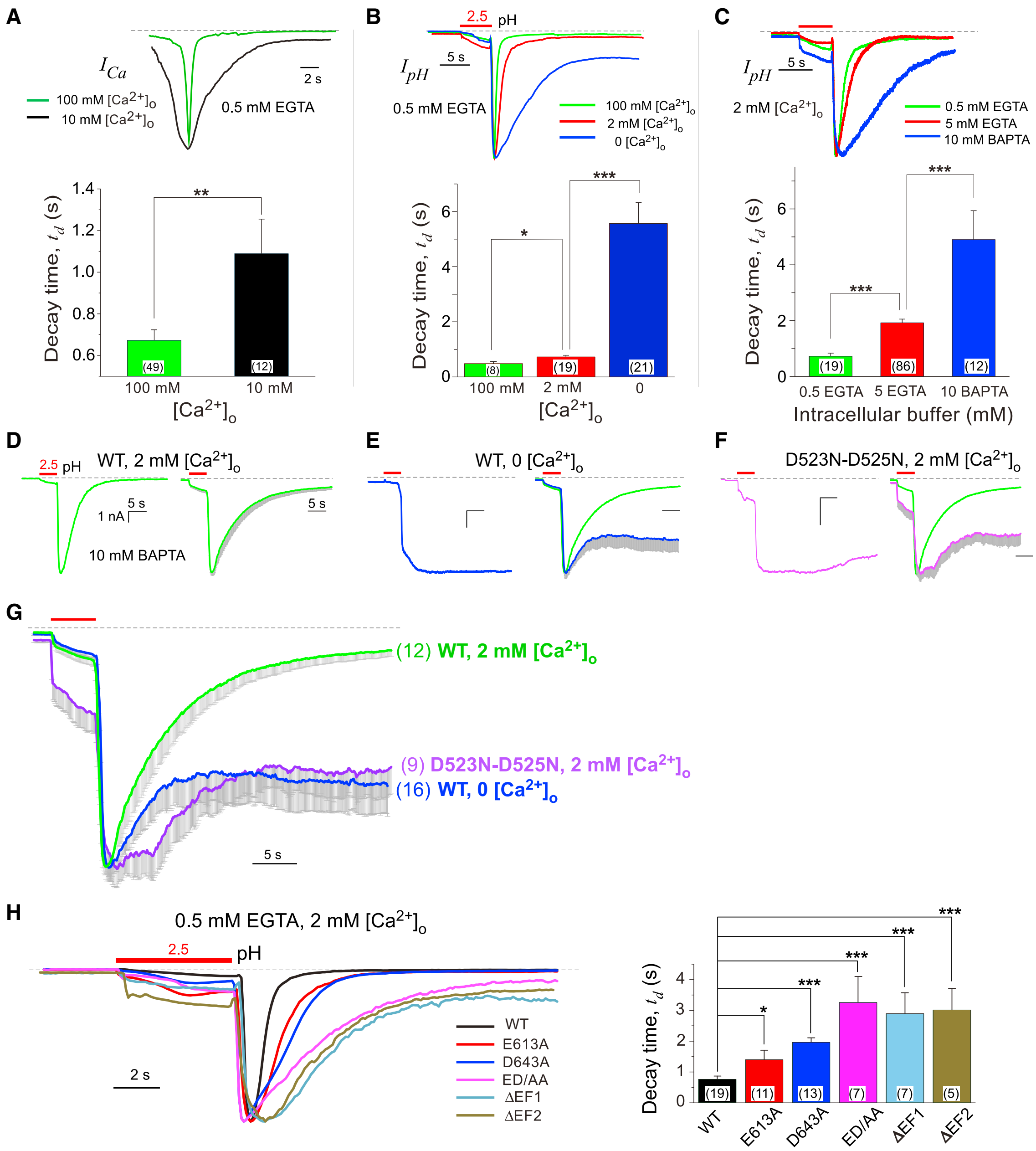

Figure 5. Ca^{2+} Dependence of Inactivation and Regulatory Roles of EF Hands

(A) Decay speed for Ca^{2+} spikes with different $[Ca^{2+}]_o$. I_{Ca} traces were normalized for comparisons: t_d for 100 mM $[Ca^{2+}]_o$ (0.66 ± 0.05 s, n = 49) and 10 mM $[Ca^{2+}]_o$ (1.17 ± 0.15 s, n = 12) (mean ± SEM, **p < 0.005).

(B) Decay speed of I_{pH} in different $[Ca^{2+}]_o$. Normalized I_{pH} traces were compared by their t_d values: 100 mM $[Ca^{2+}]_o$ (0.48 ± 0.07 s, n = 8), 2 mM $[Ca^{2+}]_o$ (0.84 ± 0.09 s, n = 19), and 0 $[Ca^{2+}]_o$ (5.56 ± 0.77 s, n = 21) (mean ± SEM, *p < 0.05).

(C) Decay speed of I_{pH} with different intracellular Ca^{2+} buffers. I_{pH} traces with 0.5 mM EGTA, 5 mM EGTA, and 10 mM BAPTA included in pipettes were compared, all with 2 mM $[Ca^{2+}]_o$ in the bath. Statistical summary of t_d values: 0.5 mM EGTA (0.84 ± 0.09 s, n = 19), 5 mM EGTA (1.95 ± 0.12 s, n = 86), and 10 mM BAPTA (4.90 ± 1.04 s, n = 12) (mean ± SEM, ***p < 0.001).

(D–G) Inactivation when eliminating intra- and/or extra-cellular Ca^{2+}. With 10 mM intracellular BAPTA, representative (left) and averaged (right) I_{pH} from WT and mutant channels, in 0 or 2 mM $[Ca^{2+}]_o$. In (E) and (F), channel inactivation was completely abolished for WT in 0 $[Ca^{2+}]_o$ (12 out of 27 cells) and for D523-N525N mutant in 2 mM $[Ca^{2+}]_o$ (ten out of 33 cells). Averaged traces of (D)–(F) are summarized and compared in (G).

(H) EF-hand mutations modulated I_{pH} decay. Normalized I_{pH} traces (left) and statistical summary of t_d (right): WT (0.84 ± 0.09 s, n = 19), E613A (1.40 ± 0.31 s, n = 11), D643A (1.96 ± 0.14 s, n = 13), E613A-D643A or ED/AA (3.26 ± 0.84 s, n = 7), ΔEF1 (2.90 ± 0.67 s, n = 7), and ΔEF2 (3.01 ± 0.69 s, n = 5) (mean ± SEM, *p < 0.05, ***p < 0.001).

See also Figure S6.

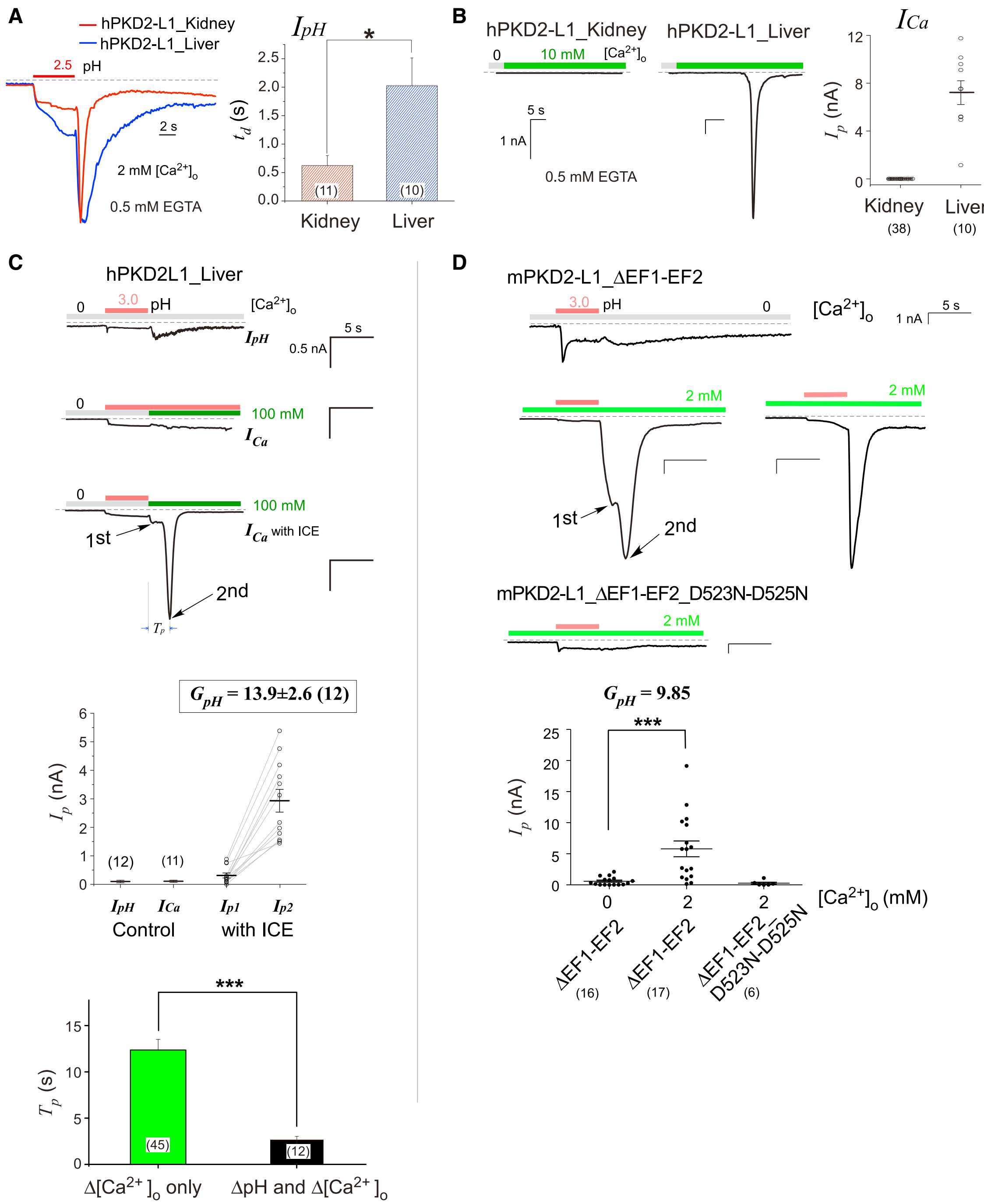

Figure 6. Manifestations of ICE with PKD2-L1 Variants and Acid Sensing

(A) Comparison for hPKD2-L1 splice variants by t_d values of I_{pH}: hPKD2-L1_Kidney (0.62 ± 0.18 s, n = 11) versus hPKD2-L1_Liver (2.02 ± 0.49 s, n = 10) (mean ± SEM, *p < 0.05). Other conditions: V_m = –60 mV, 2 mM $[Ca^{2+}]_o$ and 0.5 mM EGTA.

(B) Upon 10 mM $[Ca^{2+}]_o$ exposure, ICE spikes were evidenced from hPKD2-L1_Liver (7.2 ± 1.0 nA, n = 10) (mean ± SEM) but not from hPKD2-L1_Kidney (n = 38).

(C) ICE amplification of acid sensing with hPKD2-L1_Liver. For weak I_{pH} (pH = 3), substantial amplifications with gain factor (G_{pH}) of 13.9 ± 2.6 (n = 12) were achieved by Ca^{2+} spikes subsequent to weak I_{pH}. T_p associated with acid withdrawal was significantly shorter than that with standard I_{Ca} spikes (mean ± SEM, ***p < 0.001).

(D) ICE amplification of acid sensing with ΔEF1-EF2 mutant of mPKD2-L1. With 0 $[Ca^{2+}]_o$, weak acid of pH 3 barely produced recognizable I_{pH} (0.59 ± 0.16 nA, n = 16), in contrast to pronounced I_{pH} with 2 mM $[Ca^{2+}]_o$ (5.8 ± 1.3 nA, n = 17) (mean ± SEM, ***p < 0.001).

See also Figure S7.

OPEN ACCESS
CellPress

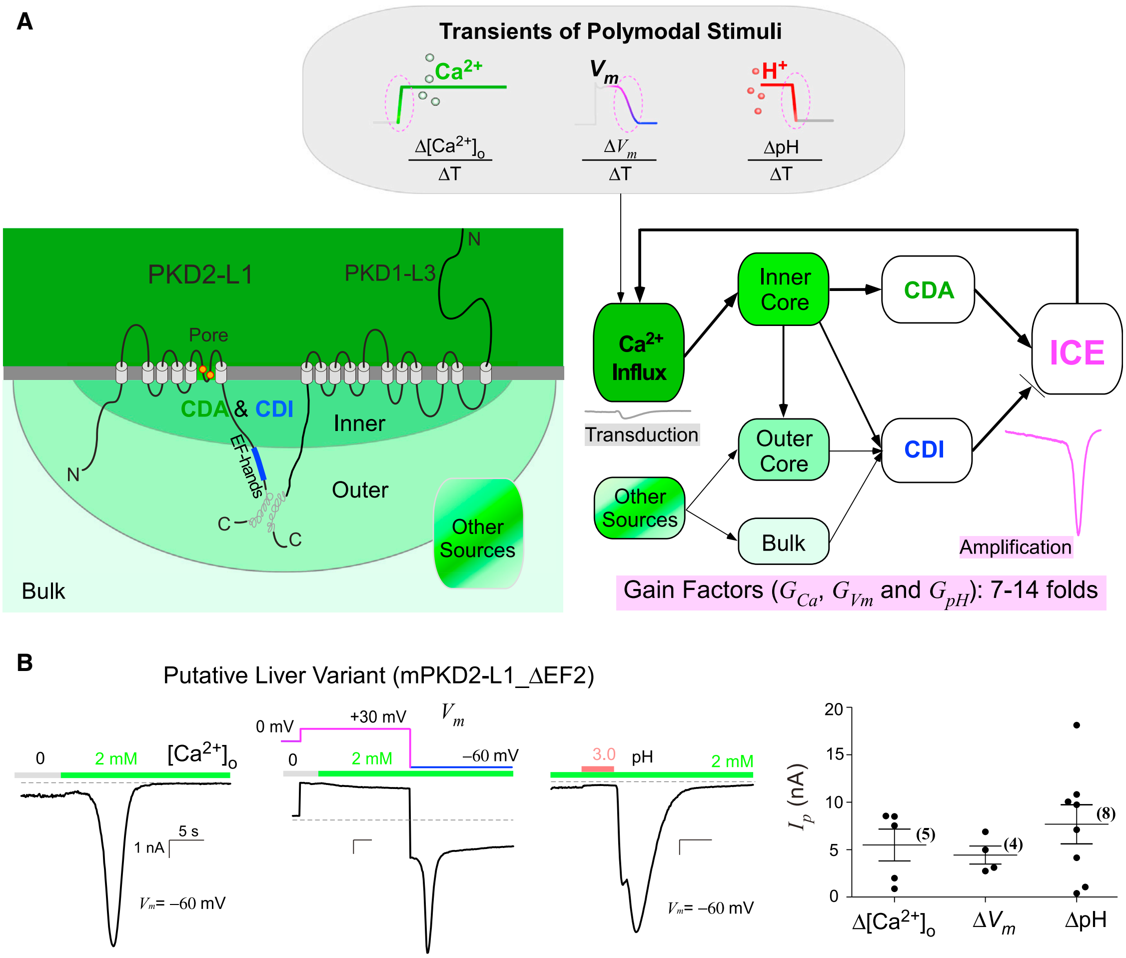

Figure 7. Scheme of ICE: Ca^{2+} Feedback Regulations and Transient Signal Facilitations

(A) Foundational scheme of ICE. Besides other sources in the cell (e.g., bulk Ca^{2+} and Ca^{2+} via other channels), Ca^{2+} nanodomain as seen by the channel is mainly created by Ca^{2+} influx through the pore of the channel and can be divided into two major subdomains (left): the inner core and the outer core. The inner core of the Ca^{2+} nanodomain associated with ICE is composed of the pore and the immediate vicinity to inner mouth of the channel. This inner core nanodomain is featured with ultrafast Ca^{2+} transients in ultrahigh concentrations and is resistant to Ca^{2+} buffers, even to a high dose of BAPTA. Ca^{2+} from the inner core is sufficient and necessary for CDA, the positive feedback with relatively fast on rate. Beyond the core, the Ca^{2+}-buffer (EGTA/BAPTA) -sensitive outer core is dynamically affected by core Ca^{2+} and other Ca^{2+} sources in the cell. Apparently opposed to CDA, Ca^{2+} also negatively regulates channels (CDI) with slower on rate than CDA. CDI is evidently mediated by Ca^{2+} core and also regulated by other sources of Ca^{2+} in the cell. EF hands of PKD2-L1 could facilitate ICE spikes once the EF hands are impaired. For channels of transduction-only mode, only small and sometimes obscure responses are produced (Figure S1); in contrast, for channels with CDI and CDA appropriately tuned, stimuli at fast rate of change ($\Delta[Ca^{2+}]_o/\Delta T$, $\Delta V_m/\Delta T$ or $\Delta pH/\Delta T$) could be amplified (7- to 14-fold) and reshaped by ICE local to individual channels.

(B) ICE spikes with putative mPKD2-L1_Liver channels. Rapid transient stimuli with physiological constraints were applied: $\Delta[Ca^{2+}]_o$ (from 0 to 2 mM), ΔV_m (with 2 mM $[Ca^{2+}]_o$ constantly present), and ΔpH (acid withdrawal from a pH of 3). mPKD2-L1_ΔEF2 channels (in complex with PKD1-L3) were capable of ICE spikes: 5.5 ± 1.7 nA (n = 5), 4. 4 ± 0.9 nA (n = 4), and 7. 7 ± 2.1 nA (n = 8), respectively (mean ± SEM).

D523N-D525N impermeable to Ca^{2+}) to acid withdrawal (averaged G_{pH}: 9.85 in response to ΔpH). Similar augmentations for stronger stimuli (pH = 2.5) were evidenced as double peaks from hPKD2-L1_Liver or mPKD2-L1_D643A (Figure S7).

DISCUSSION

The results suggest a scheme for how ICE emerges in the context of gating and signaling of the PKD2-L1/PKD1-L3 complex (Figure 7A). Ca^{2+} passing through the pore and Ca^{2+} in the immediate vicinity of the cytosolic mouth of the channel constitutes the inner core of a Ca^{2+} nanodomain sensed by the channel. Ca^{2+} in the inner core, which is present at mM concentrations (Tadross et al., 2013), is sufficient and necessary for autonomous activation (CDA). Ca^{2+} influx via neighboring Ca_V or CatCh (Figure S5) was unable to trigger CDA of PKD2-L1/PKD1-L3, suggesting the Ca^{2+} sensor for this process could be deeply buried within the pore structure and may not be accessible by Ca^{2+} diffusion from other channels. It is imperative for future investigations to look into molecular details regarding how Ca^{2+} in the core activates the channel.

PKD2-L1/PKD1-L3 is also subject to the negative feedback of CDI, by global (outer core) and/or local (inner core) Ca^{2+} (Figure 7A). Other cytosolic Ca^{2+} sources such as integrated bulk Ca^{2+} or intracellular channels potentially including PKD2-L1 itself (Sharif-Naeini et al., 2009) also contribute to CDI. CDI is a common gating feature, shared by almost all TRP channels that permeate Ca^{2+}, that acts as a self-limiting mechanism to adjust Ca^{2+} influx and Ca^{2+} homeostasis for the cell (Gordon-Shaag et al., 2008). Mechanisms underlying local and global CDI are of great interest, e.g., CaM-mediated CDI of voltage-gated Ca^{2+} channels (Dick et al., 2008). We report here that PKD2-L1/PKD1-L3 channels also exhibit both local and global forms of CDI, although they are unlikely mediated by CaM (Figure S6). EF hands participate at least in global CDI, and local CDI can be eliminated only when Ca^{2+} influx is knocked out. Further molecular details of CDI, especially of influx-operated CDI, await future investigations.

Our data suggest that CDA should require higher $[Ca^{2+}]$ than CDI, because CDI overwhelmingly persists under almost all test conditions, whereas CDA often becomes absent once Ca^{2+} or Ca^{2+} influx is reduced or impaired (e.g., Figures 2A, 3D, and 4D). Moreover, bulk cytosolic Ca^{2+} even at the resting level causes CDI; in contrast, delivery of substantial amount of Ca^{2+} to the channel by various ways, other than through Ca^{2+} influx of its own, does not trigger CDA. Meanwhile, considering the critical time period right before spike induction, CDI has slow t_d of about 5 s or more (Figure 5B), in contrast to much faster rising phase (CDA dominant) in Ca^{2+} spikes. Although future efforts are needed to quantify the detailed gating kinetics, hints from our data suggest a relatively faster transition to open states via CDA and a slower on rate for CDI, together providing the time window for Ca^{2+} spikes to possibly happen.

ICE is uniquely different from responses of other Ca^{2+}-activated TRP channels (Hofmann et al., 2003; Launay et al., 2002; Prawitt et al., 2003; Sura et al., 2012; Wang et al., 2008; Zurborg et al., 2007) in biophysical profiles. First, ICE activation is strictly local (Figures 1 and 3). ICE is still readily inducible when intracellular Ca^{2+} is strongly buffered (Figure 1) and, using alternative routes to deliver Ca^{2+} into the cell, is unable to reproduce ICE (Figure S5). Second, ICE exhibits inward rectification (Figures 1 and 2). Third, the profile of ICE blockage is unconventional as many known blockers of PKD2-L1 including Gd^{3+} and amiloride derivatives (Ishimaru et al., 2006) all failed to block ICE spikes (Figures 1 and S2). Fourth, PKD2-L1/PKD1-L3 inactivation is fully dependent on Ca^{2+}, as a rigorous form of CDI (Figure 5). Finally, EF-hand motifs play significant roles in ICE (Figures 4 and 5). It has been speculated that EF hands could mediate activation of PKD (Petri et al., 2010) or PKD2-L1 channels (Ishimaru et al., 2006; Li et al., 2002). Our data clearly demonstrate that EF hands indirectly and negatively regulate CDA by way of CDI mediated by EF hands.

Ca^{2+} influx via the pore of PKD2-L1/PKD1-L3 channels is necessary and sufficient for CDA, and also important for full-strength CDI. The importance of Ca^{2+} influx to PKD2-L1/PKD1-L3 gating is a hallmark of ICE. Considering physiological stimuli normally only induce limited Ca^{2+} entry, autonomous sensitization to gain signal amplification would be a simple and efficient strategy; localization of the CDA machinery to the inner core ensures high specificity of information encoding in space, modality, and time. Meanwhile, the decay of ICE is dominated by the process of CDI, highly sensitive to both Ca^{2+} influx and bulk Ca^{2+} in the cell, to acquire maximum speed and strength to inactivate channel activities, serving as a form of desensitization to stimuli. Thus, ICE could serve as potential mechanisms for sensory adaptation, a key physiological feature universal to diverse sensory receptors or systems (Fain, 2003).

ICE spikes essentially turn PKD2-L1/PKD1-L3 channels into a unique type of molecular transducers specific to transient sensing/amplification, i.e., particularly sensitive to the onset/offset of the stimuli (Figure 7A). Restrictions of stimuli in the time rate of change (ΔStimuli/ΔT) have been evidenced from multiple modalities: $[Ca^{2+}]_o$ (Figure 2A), V_m (Figure 2B), and pH (Inada et al., 2008). Physiological stimuli, which might be weaker or slower than experimental conditions, would sequentially act on a certain number of channels and locally induce Ca^{2+} entries, leading to ICE events at the level of individual channels. Depending on various factors including Ca^{2+} conditions and functional expression, such temporally isolated ICE might or might not exhibit Ca^{2+} spike as we observed from "synchronized" ensemble channels at the whole-cell level, but the mechanisms of action and physiological significance should stay true regardless of spike induction. Each channel could still autonomously facilitate its own signaling with similar gain factors of G_{Ca}, G_{Vm}, and G_{pH} (about 7–14, Figures 1A, 2C, and 6C). ICE synchronization and spike induction is mainly determined by the balance between CDI and CDA of the channels. The "speed dependence" of polymodal stimuli essentially constrains the kinetics of Ca^{2+} influx to ensure that CDA would win over CDI. Sensitivity to transient rather than steady-state signals/stimuli is a prominent feature intrinsic to many sensory processes. We here present an exemplar of such transient-signal amplification and also provide mechanistic insights within the context of "time window" for Ca^{2+} spikes. To consolidate above notions, we examined putative natural splice variant of mPKD2-L1_Liver with physiologically relevant stimuli, and all exhibited Ca^{2+} spikes and signal amplification, even under stringent conditions, e.g., 2 mM $[Ca^{2+}]_o$ (Figure 7B).

PKD2-L1/PKD1-L channel complexes are capable of sensing polymodal stimuli, a common feature to TRP family (Voets et al., 2005). ICE discovered herein highlights the notion that the recombinant system with overexpression under appropriate conditions (e.g., Ca^{2+}) should be an advantageous strategy to elucidate sensory transduction of candidate channels, many of which still remain unidentified. Exciting directions include the putative mechanosensitivity of cilia to the fluid flow (Delling et al., 2013; Murakami et al., 2005; Nauli et al., 2003), the unidentified mechanoelectrical transducer in hair cells (Fettiplace, 2009), the high-salt sensation in aversive taste (Oka et al., 2013), the potential involvement in calcium taste (Tordoff, 2001), and the unexplored role in Ca^{2+} signaling coupled with action potentials in cardiac myocytes or neurons (Li et al., 2007; Orts Del'Immagine et al., 2015). ICE might also involve in Ca^{2+} regulations and Ca^{2+} signaling related to PKD2-L1 pathophysiology (Barretto et al., 2015; DeCaen et al., 2013; Delling et al., 2013; Desimone et al., 2012; Djenoune et al., 2014; Huang et al., 2006; Orts-Del'Immagine et al., 2014, 2015). PKD2-L1/PKD1-L3 with ICE could segregate its Ca^{2+} signaling into divergent biological tasks by active or transduction-amplification mode versus passive or transduction-only mode (Figure 7A). Our work invites future investigations on whether and how ICE dysfunction would affect Ca^{2+} signaling related to sensory functions and neural development in PKD2-L1 expressing neurons, or Ca^{2+} homeostasis and hedgehog signaling in primary cilia.

Dysregulated PKD channels with impaired Ca^{2+} signaling would cause serious consequences as in ADPKD (Vassilev et al., 2001), or left-right determination (Yoshiba et al., 2012). TRPPs including PKD and PKD2-L1 share high homology in sequence, structure, assembly, and functionality. PKD activities exhibit a bell-shaped Ca^{2+} dependence (Cai et al., 2004; Ćelić et al., 2012; Koulen et al., 2002; Yoshiba et al., 2012), resembling the dual Ca^{2+}-dependent processes unveiled in ICE (both CDA and CDI). It is thus attractive to speculate that PKD complex might also utilize ICE-like mechanism to facilitate its transmembrane signaling. If proved, this would not only elucidate unresolved mechanisms underlying key functions of PKD, but also promise cellularly robust, physiologically relevant, and drug-screening-compatible assays aimed at potential therapeutics for this prevalent but unconquered channelopathy (Zhou, 2009).

We present here a type of Ca^{2+} influx-operated Ca^{2+} spike-like response or ICE from PKD2-L1/PKD1-L3 channel complex, which serves to augment and reshape its transmembrane signaling. ICE opens up promising avenues to understand the gating, signaling, and pathophysiology of PKD2-L1/PKD1-L3; meanwhile, as a mode of action, such autonomous ICE is expected to expand onto other channels and other modalities (Delmas, 2005; Yu and Catterall, 2004).

EXPERIMENTAL PROCEDURES

Molecular Biology

TRPP3 and PKD1-L3 of *Mus musculus* (mPKD2-L1 [GenBank: A2A259]; mPKD1-L3 [GenBank: AY164486]) were provided by Dr. H. Matsunami (Duke University). TRPP3 of *Homo sapiens* (hPKD2-L1 [GenBank: NM_016112]) were from Drs. Yong Yu (St. John's University) and Dominic Norris (Medical Research Council). CatCh was subcloned from ChR2 (Dr. Karl Deisseroth, Stanford University). Point mutations related to the pore domain or EF hands were achieved by QuikChange Lightning Site-Directed Mutagenesis Kit (Agilent Technologies). All segments subject to PCR or QuikChange were verified by sequencing. Details about cDNA constructs and molecular biology are provided in Supplemental Experimental Procedures.

Transfection of cDNA Constructs

HEK293 or CHO cells with recombinant channels were prepared according to established protocols (Liu et al., 2010). Additional cDNA constructs were applied when necessary, including GCaMP3 (from Drs. Minmin Luo and Sen Song, Tsinghua University), $Ca_V2.2$ and CaM or CaM_{1234} (from Dr. David Yue, Johns Hopkins University), and CatCh. PKD2 and PKD1 of *Homo sapiens* were generous gifts from Dr. Terry Watnick (Johns Hopkins University). PKD1-L1 of *Mus musculus* (mPKD1-L1 [GenBank: XM_126005]) were from Drs. Yong Yu (St. John's University) and Dominic Norris (Medical Research Council).

Patch-Clamp Electrophysiology

Electrodes were pulled and heat-polished, resulting in 1- to 3-MΩ resistances. Whole-cell signals were acquired and analyzed by an Axopatch 200B amplifier and the pCLAMP system (Molecular Devices). The rapid solution changer RSC-200 (Bio-Logic) was used for brief applications of acid stimulus or rapid exposure of high Ca^{2+}. Bath solutions were perfused into a recording chamber with Valve Commander ALA-VM4 (ALA Scientific Instruments). Relative permeability of Ca^{2+} versus Na^+ can be calculated from estimated reversal potentials ($V_{rev,\ Ca}$ and $V_{rev,\ Na}$) in extracellular solutions of Ca^{2+}-based (Na^+ free) or Na^+-based (Ca^{2+} free) during the spike phase (Hille, 2001; Yu et al., 2012):

$$P_{Ca}/P_{Na} = \frac{[Na^+]_o}{4[Ca^{2+}]_o} e^{\frac{F}{RT}\left(V_{rev,\ Ca}\text{-}V_{rev,\ Na}\right)}\left(e^{\frac{F}{RT}V_{rev,Ca}}+1\right).$$

Details about solutions and calculations are provided in Supplemental Experimental Procedures.

Chemicals and Reagents

Chemical compounds including phenamil, capsaicin, $GdCl_3$, and thapsigargin were all purchased from Sigma-Aldrich. These compounds were dissolved in DMSO or water at stock concentration (phenamil, capsaicin, and $GdCl_3$: 10 mM; thapsigargin: 1 mM) and then diluted by bath/electrode solutions to final working concentrations.

Fluorescence Ca^{2+} Imaging

Experiments were carried out in HEK293 cells expressing PKD1-L3, PKD2-L1 or their mutants, along with GCaMP3. Fluorescence images were acquired with a Nikon Ti-S inverted microscope with Neo sCMOS CCD at a frame interval of 1–5 s and analyzed with iQ2 software (Andor Technology).

Structure Modeling

For structure homology modeling of EF hands from mPKD2-L1, we used online website Swiss modeler (http://swissmodel.expasy.org/) and took the structure of the EF-hand domain of hPKD2 from Protein Data Bank (PDB: 2Y4Q) as the template. PyMOL was used for superimposition and inspection of the structures (DeLano Scientific).

Data Analysis and Statistics

Data were analyzed in Clampfit (Molecular Devices), Origin software (OriginLab), and Excel (Microsoft). SEM and Student's t test (two-tailed, criteria of significance: $^*p < 0.05$; $^{**}p < 0.01$; or $^{***}p < 0.001$) were calculated when applicable.

SUPPLEMENTAL INFORMATION

Supplemental Information includes Supplemental Experimental Procedures and seven figures and can be found with this article online at http://dx.doi.org/10.1016/j.celrep.2015.09.041.

AUTHOR CONTRIBUTIONS

M.H. and Y.L. performed experiments and analyses and helped prepare the manuscript. J.W. acquired data during pilot experiments and conducted preliminary analyses. X.L. conceived the project, designed the experiments, conducted analyses, and wrote the paper.

ACKNOWLEDGMENTS

We thank all the X-Lab members for discussions. We acknowledge the researchers who shared the constructs as indicated in the Experimental Procedures. We particularly thank Drs. Cecilia Canessa and Henry Colecraft for reading and editing the manuscript. We also thank Drs. Wei Yang and Peihua Chen for providing initial help in acid-evoked off responses and Drs. Bailong Xiao and Yichang Jia for reading the manuscript and providing suggestions. This work is supported by National Science Foundation of China (NSFC) grants 81171382 and 31370822; National Key Basic Research (973) Program 2011CB707701; Beijing Natural Science Foundation (BNSF) grant 7142089; and Tsinghua National Lab for Information Science and Technology (TNList) Cross-discipline Foundation, all to X.L. X.L. also received support from Tsinghua-Peking Center for Life Sciences (CLS).

Received: May 18, 2015
Revised: August 18, 2015
Accepted: September 13, 2015
Published: October 15, 2015

REFERENCES

Barretto, R.P., Gillis-Smith, S., Chandrashekar, J., Yarmolinsky, D.A., Schnitzer, M.J., Ryba, N.J., and Zuker, C.S. (2015). The neural representation of taste quality at the periphery. Nature *517*, 373–376.

Cai, Y., Anyatonwu, G., Okuhara, D., Lee, K.B., Yu, Z., Onoe, T., Mei, C.L., Qian, Q., Geng, L., Wiztgall, R., et al. (2004). Calcium dependence of polycystin-2 channel activity is modulated by phosphorylation at Ser812. J. Biol. Chem. *279*, 19987–19995.

Ćelić, A.S., Petri, E.T., Benbow, J., Hodsdon, M.E., Ehrlich, B.E., and Boggon, T.J. (2012). Calcium-induced conformational changes in C-terminal tail of polycystin-2 are necessary for channel gating. J. Biol. Chem. *287*, 17232–17240.

Chen, X.Z., Vassilev, P.M., Basora, N., Peng, J.B., Nomura, H., Segal, Y., Brown, E.M., Reeders, S.T., Hediger, M.A., and Zhou, J. (1999). Polycystin-L is a calcium-regulated cation channel permeable to calcium ions. Nature *401*, 383–386.

Chen, P., Wu, J.Z., Zhao, J., Wang, P., Luo, J., Yang, W., and Liu, X.D. (2015). PKD2L1/PKD1L3 channel complex with an alkali-activated mechanism and calcium-dependent inactivation. Eur. Biophys. J. *44*, 483–492.

DeCaen, P.G., Delling, M., Vien, T.N., and Clapham, D.E. (2013). Direct recording and molecular identification of the calcium channel of primary cilia. Nature *504*, 315–318.

Delling, M., DeCaen, P.G., Doerner, J.F., Febvay, S., and Clapham, D.E. (2013). Primary cilia are specialized calcium signalling organelles. Nature *504*, 311–314.

Delmas, P. (2005). Polycystins: polymodal receptor/ion-channel cellular sensors. Pflugers Arch. *451*, 264–276.

Desimone, J.A., Ren, Z., Phan, T.H., Heck, G.L., Mummalaneni, S., and Lyall, V. (2012). Changes in taste receptor cell [Ca2+]i modulate chorda tympani responses to salty and sour taste stimuli. J. Neurophysiol. *108*, 3206–3220.

Dick, I.E., Tadross, M.R., Liang, H., Tay, L.H., Yang, W., and Yue, D.T. (2008). A modular switch for spatial Ca2+ selectivity in the calmodulin regulation of CaV channels. Nature *451*, 830–834.

Djenoune, L., Khabou, H., Joubert, F., Quan, F.B., Nunes Figueiredo, S., Bodineau, L., Del Bene, F., Burcklé, C., Tostivint, H., and Wyart, C. (2014). Investigation of spinal cerebrospinal fluid-contacting neurons expressing PKD2L1: evidence for a conserved system from fish to primates. Front. Neuroanat. *8*, 26.

Fain, G.L. (2003). Sensory transduction (Sunderland, Mass.: Sinauer Associates).

Fettiplace, R. (2009). Defining features of the hair cell mechanoelectrical transducer channel. Pflugers Arch. *458*, 1115–1123.

Fujimoto, C., Ishimaru, Y., Katano, Y., Misaka, T., Yamasoba, T., Asakura, T., and Abe, K. (2011). The single pore residue Asp523 in PKD2L1 determines Ca2+ permeation of the PKD1L3/PKD2L1 complex. Biochem. Biophys. Res. Commun. *404*, 946–951.

Gees, M., Colsoul, B., and Nilius, B. (2010). The role of transient receptor potential cation channels in Ca2+ signaling. Cold Spring Harb. Perspect. Biol. *2*, a003962.

Gordon-Shaag, A., Zagotta, W.N., and Gordon, S.E. (2008). Mechanism of Ca(2+)-dependent desensitization in TRP channels (Austin: Channel), p. 2.

Higuchi, T., Shimizu, T., Fujii, T., Nilius, B., and Sakai, H. (2014). Gating modulation by heat of the polycystin transient receptor potential channel PKD2L1 (TRPP3). Pflugers Arch. *466*, 1933–1940.

Hille, B. (2001). Ion channels of excitable membranes, Third Edition (Sunderland, Mass.: Sinauer).

Hofmann, T., Chubanov, V., Gudermann, T., and Montell, C. (2003). TRPM5 is a voltage-modulated and Ca(2+)-activated monovalent selective cation channel. Curr. Biol. *13*, 1153–1158.

Huang, A.L., Chen, X., Hoon, M.A., Chandrashekar, J., Guo, W., Tränkner, D., Ryba, N.J., and Zuker, C.S. (2006). The cells and logic for mammalian sour taste detection. Nature *442*, 934–938.

Huque, T., Cowart, B.J., Dankulich-Nagrudny, L., Pribitkin, E.A., Bayley, D.L., Spielman, A.I., Feldman, R.S., Mackler, S.A., and Brand, J.G. (2009). Sour ageusia in two individuals implicates ion channels of the ASIC and PKD families in human sour taste perception at the anterior tongue. PLoS ONE *4*, e7347.

Inada, H., Kawabata, F., Ishimaru, Y., Fushiki, T., Matsunami, H., and Tominaga, M. (2008). Off-response property of an acid-activated cation channel complex PKD1L3-PKD2L1. EMBO Rep. *9*, 690–697.

Ishii, S., Kurokawa, A., Kishi, M., Yamagami, K., Okada, S., Ishimaru, Y., and Misaka, T. (2012). The response of PKD1L3/PKD2L1 to acid stimuli is inhibited by capsaicin and its pungent analogs. FEBS J. *279*, 1857–1870.

Ishimaru, Y., Inada, H., Kubota, M., Zhuang, H., Tominaga, M., and Matsunami, H. (2006). Transient receptor potential family members PKD1L3 and PKD2L1 form a candidate sour taste receptor. Proc. Natl. Acad. Sci. USA *103*, 12569–12574.

Kawaguchi, H., Yamanaka, A., Uchida, K., Shibasaki, K., Sokabe, T., Maruyama, Y., Yanagawa, Y., Murakami, S., and Tominaga, M. (2010). Activation of polycystic kidney disease-2-like 1 (PKD2L1)-PKD1L3 complex by acid in mouse taste cells. J. Biol. Chem. *285*, 17277–17281.

Keller, S.A., Jones, J.M., Boyle, A., Barrow, L.L., Killen, P.D., Green, D.G., Kapousta, N.V., Hitchcock, P.F., Swank, R.T., and Meisler, M.H. (1994). Kidney and retinal defects (Krd), a transgene-induced mutation with a deletion of mouse chromosome 19 that includes the Pax2 locus. Genomics *23*, 309–320.

Koulen, P., Cai, Y., Geng, L., Maeda, Y., Nishimura, S., Witzgall, R., Ehrlich, B.E., and Somlo, S. (2002). Polycystin-2 is an intracellular calcium release channel. Nat. Cell Biol. *4*, 191–197.

Launay, P., Fleig, A., Perraud, A.L., Scharenberg, A.M., Penner, R., and Kinet, J.P. (2002). TRPM4 is a Ca2+-activated nonselective cation channel mediating cell membrane depolarization. Cell *109*, 397–407.

Li, Q., Liu, Y., Zhao, W., and Chen, X.Z. (2002). The calcium-binding EF-hand in polycystin-L is not a domain for channel activation and ensuing inactivation. FEBS Lett. *516*, 270–278.

Li, Q., Dai, X.Q., Shen, P.Y., Wu, Y., Long, W., Chen, C.X., Hussain, Z., Wang, S., and Chen, X.Z. (2007). Direct binding of alpha-actinin enhances TRPP3 channel activity. J. Neurochem. *103*, 2391–2400.

Liu, X., Yang, P.S., Yang, W., and Yue, D.T. (2010). Enzyme-inhibitor-like tuning of Ca(2+) channel connectivity with calmodulin. Nature *463*, 968–972.

Murakami, M., Ohba, T., Xu, F., Shida, S., Satoh, E., Ono, K., Miyoshi, I., Watanabe, H., Ito, H., and Iijima, T. (2005). Genomic organization and functional analysis of murine PKD2L1. J. Biol. Chem. *280*, 5626–5635.

Nauli, S.M., Alenghat, F.J., Luo, Y., Williams, E., Vassilev, P., Li, X., Elia, A.E., Lu, W., Brown, E.M., Quinn, S.J., et al. (2003). Polycystins 1 and 2 mediate mechanosensation in the primary cilium of kidney cells. Nat. Genet. *33*, 129–137.

Oka, Y., Butnaru, M., von Buchholtz, L., Ryba, N.J., and Zuker, C.S. (2013). High salt recruits aversive taste pathways. Nature *494*, 472–475.

Orts-Del'Immagine, A., Kastner, A., Tillement, V., Tardivel, C., Trouslard, J., and Wanaverbecq, N. (2014). Morphology, distribution and phenotype of polycystin kidney disease 2-like 1-positive cerebrospinal fluid contacting neurons in the brainstem of adult mice. PLoS ONE *9*, e87748.

Orts Del'Immagine, A., Seddik, R., Tell, F., Airault, C., Er-Raoui, G., Najimi, M., Trouslard, J., and Wanaverbecq, N. (2015). A single polycystic kidney disease 2-like 1 channel opening acts as a spike generator in cerebrospinal fluid-contacting neurons of adult mouse brainstem. Neuropharmacology, Published online July 25, 2015. http://dx.doi.org/10.1016/j.neuropharm.2015.07.030.

Petri, E.T., Celic, A., Kennedy, S.D., Ehrlich, B.E., Boggon, T.J., and Hodsdon, M.E. (2010). Structure of the EF-hand domain of polycystin-2 suggests a mechanism for Ca2+-dependent regulation of polycystin-2 channel activity. Proc. Natl. Acad. Sci. USA *107*, 9176–9181.

Prawitt, D., Monteilh-Zoller, M.K., Brixel, L., Spangenberg, C., Zabel, B., Fleig, A., and Penner, R. (2003). TRPM5 is a transient Ca2+-activated cation channel responding to rapid changes in [Ca2+]i. Proc. Natl. Acad. Sci. USA *100*, 15166–15171.

Sharif-Naeini, R., Folgering, J.H.A., Bichet, D., Duprat, F., Lauritzen, I., Arhatte, M., Jodar, M., Dedman, A., Chatelain, F.C., Schulte, U., et al. (2009). Polycystin-1 and -2 dosage regulates pressure sensing. Cell *139*, 587–596.

Shimizu, T., Janssens, A., Voets, T., and Nilius, B. (2009). Regulation of the murine TRPP3 channel by voltage, pH, and changes in cell volume. Pflugers Arch. *457*, 795–807.

Sura, L., Zíma, V., Marsakova, L., Hynkova, A., Barvík, I., and Vlachova, V. (2012). C-terminal acidic cluster is involved in Ca2+-induced regulation of human transient receptor potential ankyrin 1 channel. J. Biol. Chem. *287*, 18067–18077.

Tadross, M.R., Tsien, R.W., and Yue, D.T. (2013). Ca2+ channel nanodomains boost local Ca2+ amplitude. Proc. Natl. Acad. Sci. USA *110*, 15794–15799.

Tang, L., Gamal El-Din, T.M., Payandeh, J., Martinez, G.Q., Heard, T.M., Scheuer, T., Zheng, N., and Catterall, W.A. (2014). Structural basis for Ca2+ selectivity of a voltage-gated calcium channel. Nature *505*, 56–61.

Tordoff, M.G. (2001). Calcium: taste, intake, and appetite. Physiol. Rev. *81*, 1567–1597.

Vassilev, P.M., Guo, L., Chen, X.Z., Segal, Y., Peng, J.B., Basora, N., Babakhanlou, H., Cruger, G., Kanazirska, M., Ye Cp, et al. (2001). Polycystin-2 is a novel cation channel implicated in defective intracellular Ca(2+) homeostasis in polycystic kidney disease. Biochem. Biophys. Res. Commun. *282*, 341–350.

Voets, T., Talavera, K., Owsianik, G., and Nilius, B. (2005). Sensing with TRP channels. Nat. Chem. Biol. *1*, 85–92.

Wang, Y.Y., Chang, R.B., Waters, H.N., McKemy, D.D., and Liman, E.R. (2008). The nociceptor ion channel TRPA1 is potentiated and inactivated by permeating calcium ions. J. Biol. Chem. *283*, 32691–32703.

Wu, G., Hayashi, T., Park, J.H., Dixit, M., Reynolds, D.M., Li, L., Maeda, Y., Cai, Y., Coca-Prados, M., and Somlo, S. (1998). Identification of PKD2L, a human PKD2-related gene: tissue-specific expression and mapping to chromosome 10q25. Genomics *54*, 564–568.

Yoshiba, S., Shiratori, H., Kuo, I.Y., Kawasumi, A., Shinohara, K., Nonaka, S., Asai, Y., Sasaki, G., Belo, J.A., Sasaki, H., et al. (2012). Cilia at the node of mouse embryos sense fluid flow for left-right determination via Pkd2. Science *338*, 226–231.

Yu, F.H., and Catterall, W.A. (2004). The VGL-chanome: a protein superfamily specialized for electrical signaling and ionic homeostasis. Sci. STKE *2004*, re15.

Yu, Y., Ulbrich, M.H., Li, M.H., Dobbins, S., Zhang, W.K., Tong, L., Isacoff, E.Y., and Yang, J. (2012). Molecular mechanism of the assembly of an acid-sensing receptor ion channel complex. Nat. Commun. *3*, 1252.

Zheng, W., Hussein, S., Yang, J., Huang, J., Zhang, F., Hernandez-Anzaldo, S., Fernandez-Patron, C., Cao, Y., Zeng, H., Tang, J., and Chen, X.Z. (2015). A novel PKD2L1 C-terminal domain critical for trimerization and channel function. Sci. Rep. *5*, 9460.

Zhou, J. (2009). Polycystins and primary cilia: primers for cell cycle progression. Annu. Rev. Physiol. *71*, 83–113.

Zurborg, S., Yurgionas, B., Jira, J.A., Caspani, O., and Heppenstall, P.A. (2007). Direct activation of the ion channel TRPA1 by Ca2+. Nat. Neurosci. *10*, 277–279.